

Particle Size Distribution Modification During and After Electrical Charging: Comparison between a Corona Ionizer and a Radioactive Neutralizer

M. Alonso*, F.J. Alguacil

*National Center for Metallurgical Research (CSIC) Avenida Gregorio del Amo,
8. 28040 Madrid, Spain*

Abstract

This article presents the results of an experimental investigation carried out to examine the changes of the size distribution of ultrafine particles that take place in aerosol electrical chargers. Two types of commercially available chargers have been studied: an unipolar corona discharge ionizer, and a bipolar radioactive neutralizer. Particle diffusion losses to the walls modify the size distribution in both chargers to approximately the same extent. Additionally, particles can grow by Brownian coagulation in the radioactive neutralizer if the aerosol particle number concentration is above about $10^7/\text{cm}^3$. In contrast, the extremely small volume of the corona ionizer used in the experiments, 2 cm^3 , prevents coagulation even when the aerosol concentration is very high. For particle number concentration above $10^7/\text{cm}^3$ aerosol coagulation takes place downstream of any of these two chargers. The experimental results have been compared with those obtained by numerical integration of the population balance equations including charging, coagulation and diffusion losses. In spite that the coagulation rate between charged particles of opposite polarity is one to two orders of magnitude larger than the corresponding rate for uncharged particles, the numerical calculations have shown that the expected electrostatic enhancement of coagulation is negligible, probably because the fraction of charged particles in the radioactive neutralizer is too low for the particle size range studied.

Keywords: Aerosol charging; Coagulation; Nanoparticle measurement.

INTRODUCTION

It is important to quantify the changes in the aerosol particle size distribution that occur in an electric charger, specially when

the charging process constitutes a previous step to perform size distribution measurements by mobility analysis. If there is no condensing species in the charger, these changes are brought about by particle losses to the wall and Brownian coagulation. In turn, particle losses can take place by Brownian diffusion, electrostatic dispersion

*Corresponding author:

E-mail address: malonso@cenim.csic.es

(space-charge), and, if there is an external electric field, by electrostatic deposition as well.

The extent to which any of the above mentioned particle loss mechanisms occur depends on the type of charger. Chargers may be classified into two main types: unipolar and bipolar chargers. In principle, one expects negligible particle losses by electrostatic dispersion in bipolar chargers and, at the same time, larger coagulation rates because of electrostatic attraction between charged particles of opposite sign. In comparison, the particle size growth rate in unipolar chargers should be smaller since the fraction of unipolarly charged particles can be very high; for instance, practically all the particles with diameter above 15 nm can acquire a charge of the same sign in the corona ionizer we have used in this work. However, unipolar chargers are prone to produce large losses either by electrostatic dispersion or, if ions are generated by corona discharge, by direct electrostatic precipitation.

Diffusion losses may be reduced by using a stream of sheath air surrounding the aerosol stream, as was done by Chen and Pui (1999). However, the benefit of reducing particle loss is gained at the expense of diluting the aerosol, which may be a disadvantage if the ultimate objective is to generate high concentration of charged particles. Several types of unipolar chargers have been developed. In some of them a radioactive source is used to generate bipolar ions, from which those with the

desired polarity are separated by means of an electric field (Adachi *et al.*, 1985; Wiedensohler *et al.*, 1994; Chen and Pui, 1999). In others, the ions are generated by corona discharge (Buscher *et al.*, 1994; Kruis & Fissan, 2001; Hernández-Sierra *et al.*, 2003; Qi *et al.*, 2007; Qi *et al.*, 2008). As for bipolar chargers, the most widely used are radioactive chargers, also called neutralizers, which generally consist of a cylinder containing a radioactive substance, such as ^{241}Am , ^{85}Kr , ^{210}Po , etc.

In the present work, we have examined how the particle size distribution is modified as the aerosol passes through the charger. Comparative measurements have been done for two types of charger: a ^{85}Kr neutralizer, and a unipolar corona discharge ionizer.

EXPERIMENTAL

Fig. 1 shows the flow diagram of the experimental setup used to examine the particle size distribution modification inside the chargers. An evaporation-condensation NaCl aerosol, diluted by passing a desired fraction of it through an absolute filter, was electrically charged in either a corona ionizer or a ^{85}Kr neutralizer. The mobility distribution of the aerosol was measured with a differential mobility analyzer (DMA, TSI short column) and a condensation nucleus counter (TSI 3025). The aerosol flow rate through the system was kept fixed at 2 L/min. The DMA was operated in open mode with a sheath air flow rate (= excess) of 20 L/min. The radioactive neutralizer

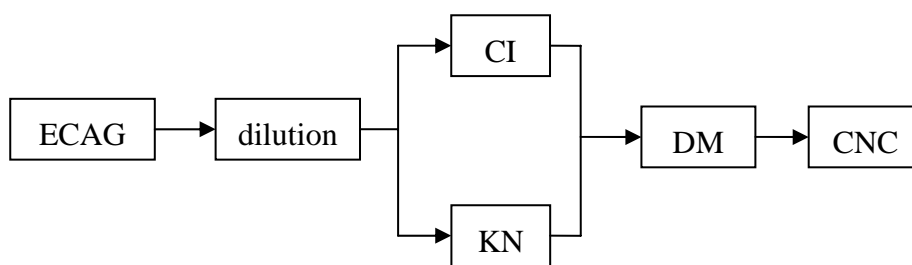


Fig. 1. Flow diagram of the experimental setup for measurement of the particle size distribution modification inside the chargers. ECAG = evaporation-condensation aerosol generator; CI = corona ionizer; KN = ^{85}Kr neutralizer; DMA = differential mobility analyzer; CNC = condensation nucleus counter.

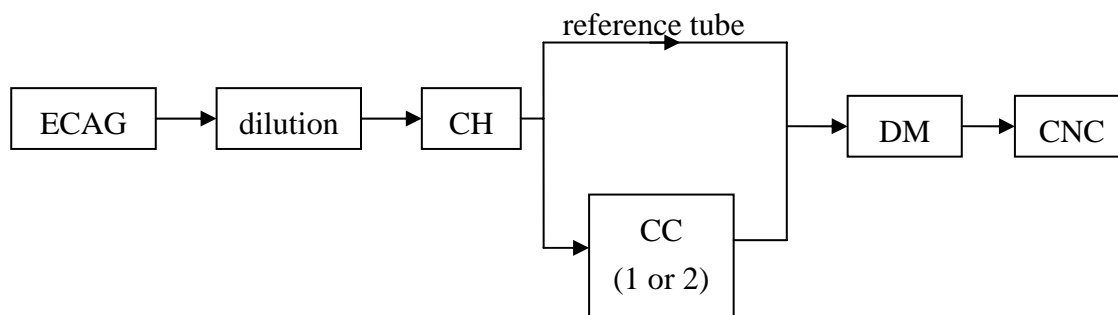


Fig. 2. Flow diagram of the experimental setup for the measurement of the particle size distribution modification downstream of the chargers. ECAG = evaporation-condensation aerosol generator; CH = ^{85}Kr neutralizer or corona ionizer; CC = coagulation chamber; DMA = differential mobility analyzer; CNC = condensation nucleus counter.

employed was the TSI model 3077. The corona ionizer was the IONER model CC08010, whose performance evaluation has been described elsewhere (Alguacil and Alonso, 2006; Alonso *et al.*, 2006). It consists of an inner stainless steel electrode ending in a sharp tip, coaxial with a grounded metal cylinder whose inner wall has a conical shape. The distance between the corona electrode tip and the cone apex is 1.75 mm. The corona charger was operated in positive polarity for all the experiments, at a fixed voltage of 3.4 kV; under these

conditions the *nt*-product was estimated to be around $3 \times 10^7 \text{ s/cm}^3$ (Alonso *et al.*, 2006).

Fig. 2 shows the flow diagram of the experimental setup used to examine the particle size distribution modification downstream of the chargers. Experiments for the ^{85}Kr neutralizer and for the corona ionizer were done separately. The reference tube consisted of a 4 mm ID Tygon[®] tube, very short (2 cm), to minimize losses and coagulation between the charger and the DMA. In this manner, the particle size

distribution measured when the aerosol was passed through the reference tube could be taken to be identical to that at the outlet of the charger. The coagulation chamber was simply a 32 mm ID cylinder, 118 mm in length, with tapered ends. The mean aerosol residence time in the coagulation chamber was 2.3 s. Experiments were performed with one or two identical coagulation chambers in series (mean aerosol residence times 2.3 and 4.6 s, respectively).

RESULTS AND DISCUSSION

Particle losses inside the chargers

Besides coagulation, size-dependent particle losses to the wall can also modify the aerosol particle size distribution. In the case of the corona ionizer, losses are due to three mechanisms, namely, Brownian diffusion, direct electrostatic deposition (driven by the applied electric field), and electrostatic dispersion or mutual repulsion between the unipolarly charged particles that are generated during the charging process. Diffusion losses can be easily measured, independently of the other two mechanisms, by employing a neutral monodisperse aerosol and keeping the corona voltage switched off. In contrast, it is not easy to measure separately the two electrostatic contributions to particle losses: in order to generate charged particles, an electric field must be applied and this causes the direct electrostatic deposition mechanism to appear; simultaneously, the presence of unipolarly charged particles,

which are generally in quite high concentrations inside the ionizer, results in their deposition to the walls by space-charge repulsion. It is possible, however, to measure the total electrostatic loss in the charger; a possible method has been described in detail in Alonso *et al.* (2006). In practice, the situation is still more complex: when the charger is operating, i.e. when the corona electric field is applied, diffusion losses are smaller than when the charger is switched off, because part of the particles that “should be lost by diffusion” have already been lost by any of the two electrostatic mechanisms. Clearly, when the charger is turned on, the three mechanisms act simultaneously and interdependently, in such a manner that the actual diffusion loss must be measured as the difference between the total loss and the combined electrostatic loss.

In the case of the radioactive neutralizer, Brownian diffusion is the only mechanism for particle loss, and can be readily measured by using a neutral monodisperse aerosol.

Fig. 3 shows diffusion losses as a function of particle size for the two chargers employed in the present work and aerosol flow rate of 2 L/min. Surprisingly, the results are almost coincident for both chargers, in spite that the mean aerosol residence times differ by a factor of 75 (the corona ionizer has an effective volume of 2 cm³, while the radioactive charger volume is 150 cm³). Certainly, the geometry of the corona charger, specially its entrance zone,

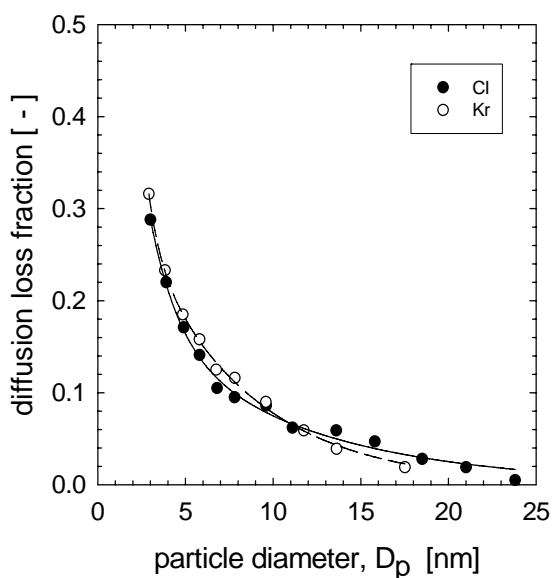


Fig. 3. Diffusion losses in the chargers for aerosol flow rate of 2 L/min. CI = corona ionizer; Kr = ^{85}Kr neutralizer.

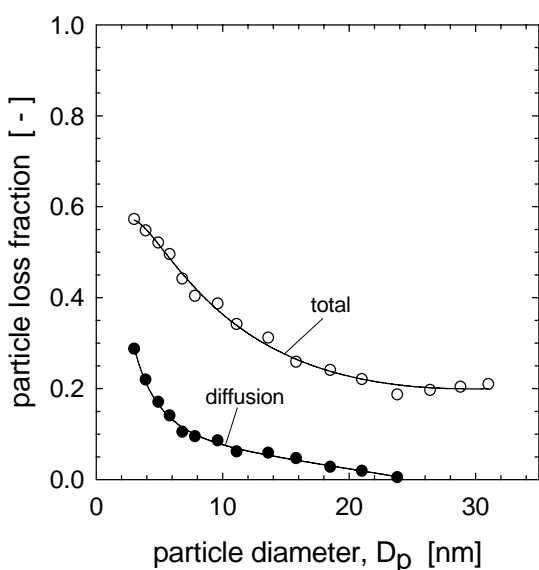


Fig. 4. Particle diffusion loss and total loss (diffusional + electrostatic) as a function of particle size for the corona ionizer operated at 3.4 kV and aerosol flow rate of 2 L/min.

is more complex than that of the radioactive neutralizer, which is a plain tube containing

an inner smaller tube, and this might explain this rather unexpected result.

Fig. 4 shows the total particle loss in the corona ionizer as a function of particle size. For comparison, the diffusion losses (same as in Fig. 3) are also plotted. As seen, the combined electrostatic losses (total minus diffusion) can be quite high. The results shown in this plot are for the specific case of corona voltage 3.4 kV and aerosol flow rate of 2 L/min.

Coagulation inside the chargers

A set of experiments were carried out using the same aerosol (i.e. keeping fixed the evaporation-condensation generator conditions) and varying the total particle number concentration by dilution. The CNC-measured concentrations were corrected to account for (i) CNC counting efficiency (Wiedensohler *et al.*, 1997); (ii) diffusion losses in the connecting tubes, using the equation of Gormley and Kennedy (1949); and (iii) particle penetration through DMA, previously measured using the technique described in Kousaka *et al.* (2000). Fig. 5 shows the size distribution of the positively charged particles at the outlet of the ^{85}Kr neutralizer, at four different levels of aerosol concentration. The particle number concentrations that appear in the legend of the plot were estimated from the size distribution measured for the corona ionizer, applying the above mentioned corrections and, additionally, taking into account the extrinsic charging efficiencies measured in a previous work (Alonso *et al.*,

2006). (Note that the use of the extrinsic charging efficiency implies that we are including all the particle losses, diffusional and electrostatic, that occur in the corona ionizer.) The distributions in Fig. 5 are presented as normalized particle number densities, so that the area under each curve is one. The plot clearly reveals that the aerosol grows by coagulation in the neutralizer when the particle number concentration is above about $2 \times 10^7 / \text{cm}^3$. For the lowest concentration, the size distribution at the neutralizer outlet practically coincides with that measured at

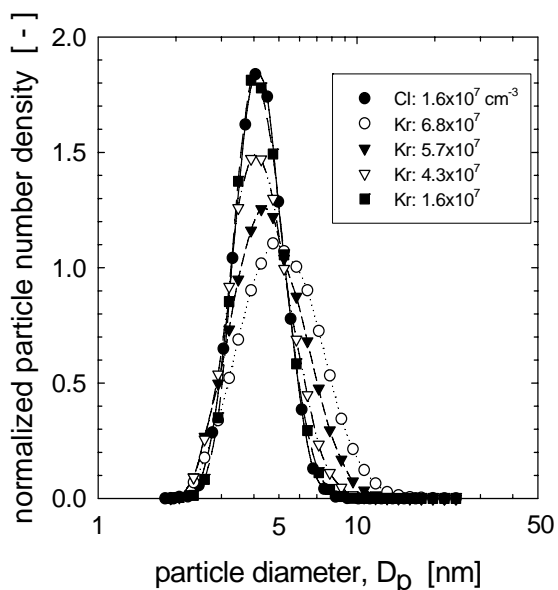


Fig. 5. Size distribution of positively charged particles measured at the outlet of the ^{85}Kr neutralizer (Kr), for different values of the total aerosol particle number concentration at the charger inlet. Comparison with the size distribution of positively charged particles measured at the outlet of the corona ionizer (CI).

the outlet of the unipolar charger (CI). The reproducibility of these results was fairly good: the differences between the geometric mean diameters obtained in three sets of experiments were less than 2%.

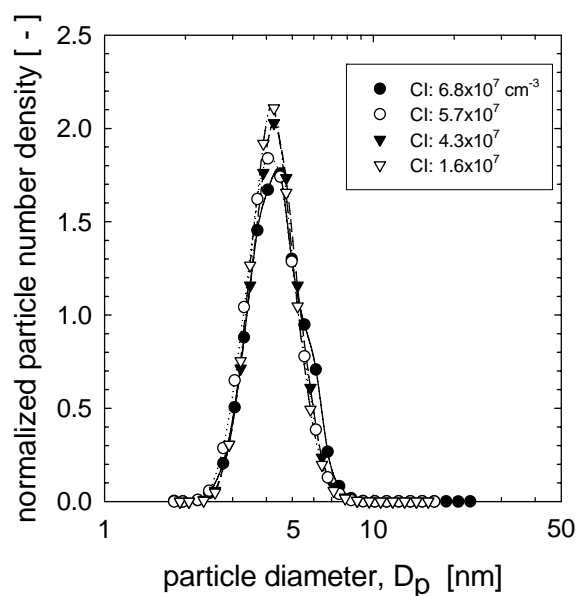


Fig. 6. Size distribution of positively charged particles measured at the outlet of the corona ionizer, for different values of the total aerosol particle number concentration at the charger inlet.

In contrast, as seen in Fig. 6, coagulation in the corona ionizer is negligible, except perhaps in the case of the largest concentration tested: the peak of the normalized distribution obtained for $6.8 \times 10^7 / \text{cm}^3$ is a bit lower than the others and the distribution is correspondingly a little broader. However, the difference is not significant. The reason for the absence of coagulation in the corona charger is its very small volume (2 cm^3) so that the mean aerosol residence time is also very small,

0.06s at aerosol flow rate of 2 L/min, that is, about 75 times smaller than for the TSI 3077 neutralizer.

Numerical calculations for the TSI neutralizer were carried out using the charging-coagulation equations as described in a former article (Alonso *et al.*, 1998):

$$\begin{aligned} \frac{dN_j^0}{dt} = & \eta_j^{+-} n N_j^- + \eta_j^{-+} n N_j^+ - \eta_j^{-0} n N_j^0 \\ & - \eta_j^{+0} n N_j^0 + \Delta \ln D_p \sum_{i=1}^{j-1} \frac{1}{2} K_{i,j-i} N_i^0 N_{j-i}^0 \\ & + \Delta \ln D_p \sum_{i=1}^{j-1} K'_{i,j-i} N_i^+ N_{j-i}^- \\ & - \Delta \ln D_p \sum_{i=1}^{\infty} K_{i,j} N_j^0 (N_i^0 + N_i^- + N_i^+) \end{aligned} \quad (1)$$

$$\begin{aligned} \frac{dN_j^+}{dt} = & \eta_j^{+0} n N_j^0 - \eta_j^{-+} n N_j^+ \\ & + \Delta \ln D_p \sum_{i=1}^{j-1} K_{i,j-i} N_i^0 N_{j-i}^+ \\ & - \Delta \ln D_p \sum_{i=1}^{\infty} N_j^+ (K_{i,j} N_i^0 + K'_{i,j} N_i^-) \end{aligned} \quad (2)$$

$$\begin{aligned} \frac{dN_j^-}{dt} = & \eta_j^{-0} n N_j^0 - \eta_j^{+-} n N_j^- \\ & + \Delta \ln D_p \sum_{i=1}^{j-1} K_{i,j-i} N_i^0 N_{j-i}^- \\ & - \Delta \ln D_p \sum_{i=1}^{\infty} N_j^- (K_{i,j} N_i^0 + K'_{i,j} N_i^+) \end{aligned} \quad (3)$$

$N_j^0 \Delta \ln D_p$, $N_j^+ \Delta \ln D_p$ and $N_j^- \Delta \ln D_p$ are, respectively, the number concentration of uncharged, positive and negative particles

with diameter in the range between D_{p_j} and

$D_{p_j} + \Delta \ln D_p$; $\eta_j^{\mu\nu}$ is the attachment rate coefficient between an ion of polarity μ and a particle of polarity ν and size D_{p_j} ; n is

the ion number concentration, assumed to be independent of its polarity and constant throughout the charging process, that is, it is assumed that the ion concentration is much larger than that of aerosol particles. $K_{i,j}$ is the coagulation rate constant between particles of diameters D_{p_i} and D_{p_j} in the case that at most one of the colliding particles is charged. $K'_{i,j}$ is the rate constant

for the coagulation of two charged particles of opposite polarity. The coagulation between charged particles of equal polarity is neglected because the corresponding rate constant is extremely low. In the above equations, the size index $j-i$ denotes particles with diameter $D_{p_{j-i}} = (D_{p_j}^3 - D_{p_i}^3)^{1/3}$.

All the aerosol particles entering the charger are uncharged. Furthermore, we assume that the initial aerosol particle size distribution is a log-normal distribution with geometric mean D_{pg} and geometric standard deviation σ_g . Therefore, the initial condition for the above system of differential equations can be expressed as

$$N_j^0 = \frac{N_0}{\sqrt{2\pi \ln \sigma_g}} \exp\left[-\frac{\ln^2(D_{pj}/D_{pg})}{2 \ln^2 \sigma_g}\right] \quad \text{and}$$

$$N_j^+ = N_j^- = 0 \quad \text{at} \quad t = 0 \quad (4)$$

where $N_0 = \Delta \ln D_p \sum_{j=1}^{\infty} [N_j^0]_{t=0}$ is the total

aerosol number concentration at the charger inlet.

The attachment coefficients were evaluated using Fuchs theory, with ionic masses of 150 and 80 amu for positive and negative ions, respectively, and corresponding mobilities of 1.15 and 1.65 cm²/Vs (Alonso *et al.* 1997).

As for the coagulation rate constants, we have used the expression due to Fuchs (Flagan and Seinfeld, 1988)

$$K_{i,j} = 2\pi(D_i + D_j)(D_{pi} + D_{pj}) \times \left[\frac{D_{pi} + D_{pj}}{D_{pi} + D_{pj} + 2g_{ij}} + \frac{8(D_i + D_j)}{c_{ij}(D_{pi} + D_{pj})} \right]^{-1} \quad (5)$$

when at least one of the coagulating particles is uncharged. (It is assumed that the presence of a charge in one of the particles does not affect the coagulation rate.) In

equation (5), $c_{ij} = (c_i^2 + c_j^2)^{1/2}$ where

$$c_j = \sqrt{8kT/\pi m_j} \quad (6)$$

is the mean thermal speed of the particle of

size D_{pj} ($k =$ Boltzmann's constant; $T =$

absolute temperature; the particle mass m_j

has been evaluated assuming spherical particles of density 2 g/cm³),

$$g_{ij} = (g_i^2 + g_j^2)^{1/2} \quad (7)$$

$$g_i = \frac{1}{3D_{pi}l_i} \left[(D_{pi} + l_i)^3 - (D_{pi}^2 + l_i^2)^{3/2} \right] - D_{pi} \quad (8)$$

$$\text{and} \quad l_i = \frac{8D_i}{\pi c_i} \quad (9)$$

is the particle mean free path. Finally, D_i is the particle diffusion coefficient.

In the case of coagulation between charged particles of opposite polarity, the rate constant has been evaluated by means of the equation (Zebel, 1966)

$$K'_{i,j} = \frac{\lambda_{i,j}}{1 - e^{-\lambda_{i,j}}} K_{i,j} \quad (10)$$

$$\text{with} \quad \lambda_{i,j} = \frac{e^2}{2\pi\epsilon_0 kT (D_{pi} + D_{pj})} \quad (11)$$

where e is the elementary charge and ϵ_0 the dielectric constant of the medium.

The system of equations (1)-(3) with initial condition (4) has been solved using a simple forward integration scheme. The particle size range of interest was subdivided in 100 intervals of constant width $\Delta \ln D_p$;

the time step for integration was taken as $\Delta t = 0.001$ s. The size distribution of the original aerosol entering the chargers were assumed to be log-normal, with a total particle number concentration estimated as above, i.e. after accounting for CNC counting efficiency, and particle losses in the connecting tubes, in the DMA and in the charger. The geometric standard deviation of the original distribution was inferred from the measurements done with the corona ionizer after consideration of total particle losses (diffusion and electrostatic) because in this case, as we have seen, there is practically no coagulation.

The comparison between experimental and numerical results are shown in Table 1. Four different calculations were carried out,

denoted as A, B, C and D in the Table. The results given in column A were obtained with the charging-coagulation equations using a coagulation rate constant dependent on particle size but not on the charging state of the particles, that is, without considering the coagulation enhancement brought about by encounters between charged particles of opposite polarity. Column B lists the results obtained when particle charge is taken into account to calculate the coagulation rate constant. As seen, the numerical results of columns A and B are identical: there is no electrostatic enhancement of coagulation. A possible reason for this surprising result is that the fraction of charged particles is too low (for 4-5 nm particles the fraction of charged particles in the bipolar neutralizer is

Table 1. Size distribution of positively charged particles at the ^{85}Kr neutralizer outlet. Comparison between experimental results and numerical calculations under various conditions. D_{pg} = geometric mean diameter; σ_g = geometric standard deviation; N_0 = aerosol particle number concentration at the charger inlet; N'_0 = corrected aerosol particle number concentration accounting for space-charge loss between the corona ionizer and the DMA.

Legend:

Column		Electrostatic enhancement of coagulation	Diffusion loss in neutralizer				Space-charge loss between corona ionizer and DMA			
A		NO	NO				NO			
B		YES	NO				NO			
C		YES	YES				NO			
D		YES	YES				YES			

N_0 cm^{-3}	N'_0 cm^{-3}	exp	D_{pg} (nm)				σ_g (-)				
			A	B	C	D	exp	A	B	C	D
6.8×10^7	1.1×10^8	4.93	4.57	4.57	4.68	4.77	1.40	1.27	1.27	1.26	1.27
5.7×10^7	8.0×10^7	4.56	4.30	4.30	4.40	4.44	1.34	1.24	1.24	1.24	1.24
4.3×10^7	5.4×10^7	4.33	4.23	4.23	4.32	4.34	1.28	1.23	1.23	1.22	1.23
1.6×10^7	1.7×10^7	4.11	4.10	4.10	4.19	4.19	1.23	1.21	1.21	1.20	1.20

of the order of 1% for each polarity). In any case, the equations underpredict both the mean particle size and the distribution width. An improvement was sought by including diffusion losses in the equations using the Gormley-Kennedy equation and assuming the neutralizer to be an empty cylinder, i.e. neglecting the presence of the inner tube containing the ^{85}Kr source. The thus obtained results (column C) are better, but still far from the experimental ones. As a final trial, we considered space-charge losses to recalculate the total aerosol concentration at the charger inlet. As explained earlier, concentrations were estimated using the data obtained for the corona ionizer; hence, it is possible that the unipolarly charged particles undergo the process of electrostatic dispersion in the tubes connecting the corona ionizer and the DMA. The recalculated concentrations are denoted as N'_0 in the Table, and the predicted particle size distribution parameters, D_{pg} and σ_g , are shown in columns D. Again, a slight improvement of the numerical results can be observed, but not enough. From the comparison, we are tempted to conclude that the actual free molecule regime coagulation rate constant is larger than the theoretical one. (It will be seen later that the predictions are better for larger particle size.)

Coagulation downstream of the chargers

Finally, we have also examined the particle size distribution modification that

can take place once the aerosol has left the charger. In practice, this does not represent a problem, because one usually shortens as much as possible the tube connecting the charger and the immediately next equipment. Nevertheless, we have undertaken this study for the sake of completeness. For these experiments, we have used an aerosol with a larger mean particle diameter and broader distribution, with particle diameters up to about 40 nm, so that we are now, at least partially, in the lower end of the transition regime, and not solely in the free molecule regime as in the experiments described in the preceding section.

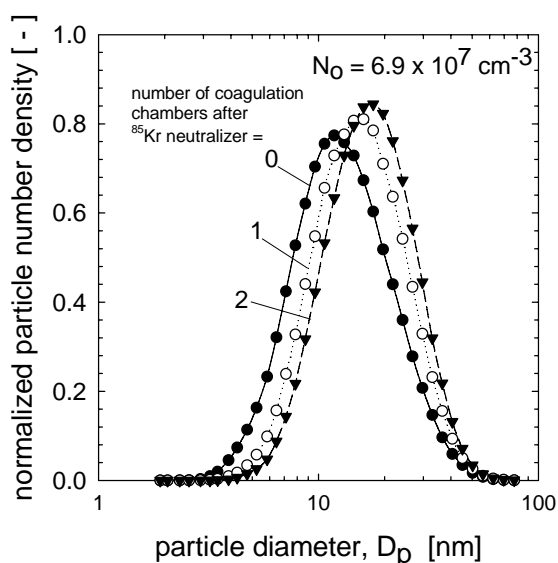


Fig. 7. Size distribution of positively charged particles after the aerosol has passed through 0, 1 and 2 coagulation chambers placed downstream of the ^{85}Kr neutralizer. Total aerosol particle number concentration at the neutralizer outlet: $6.9 \times 10^7 / \text{cm}^3$.

The experimental results for the TSI neutralizer are shown in Fig. 7, 8 and 9. The N_0 appearing in the legends of the figures denotes the total aerosol particle number concentration at the outlet of the charger, and it has been estimated as described before, i.e. accounting for CNC counting efficiency, diffusion losses in DMA and connecting tubes, and charging probability of the neutralizer. One can see again that coagulation occurs for aerosol concentration above about $10^7/\text{cm}^3$. The comparison between the experimental results and those obtained by numerical integration of the coagulation equations is shown in Table 2.

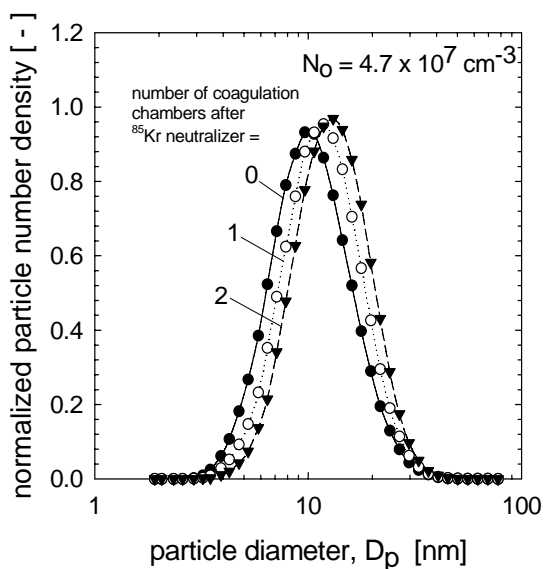


Fig. 8. Size distribution of positively charged particles after the aerosol has passed through 0, 1 and 2 coagulation chambers placed downstream of the ^{85}Kr neutralizer. Total aerosol particle number concentration at the neutralizer outlet: $4.7 \times 10^7 / \text{cm}^3$.

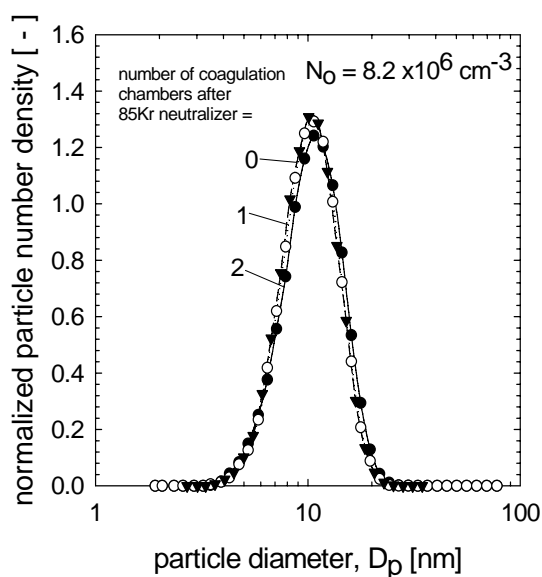


Fig. 9. Size distribution of positively charged particles after the aerosol has passed through 0, 1 and 2 coagulation chambers placed downstream of the ^{85}Kr neutralizer. Total aerosol particle number concentration at the neutralizer outlet: $8.2 \times 10^6 / \text{cm}^3$.

The matching between theory and experiments is fairly good, specially for the case of two coagulation chambers downstream of the neutralizer. As before, though the corresponding results are not included in the Table, we have found no electrostatic enhancement of coagulation, even though in the present case the fraction of charged particles is larger because particle size is also larger.

The experimental results for the corona charger are shown in Fig. 8, 9 and 10, for three levels of aerosol concentration. Note that in this case the system contains neutral particles and positively charged ones, whereas in the former case one had neutral and bipolarly charged particles. Furthermore,

the fraction of charged particles downstream of the corona ionizer is much larger than for the ^{85}Kr neutralizer. This is probably the reason why coagulation beyond the corona ionizer takes place to a slightly lesser extent. The corresponding numerical results are shown in Table 3 along with the experimental ones. The agreement between them is quite good.

An overall comparison between the numerical results discussed in this section and those of the preceding one reveals that the theoretical predictions are fairly good only for particle size above about 10 nm.

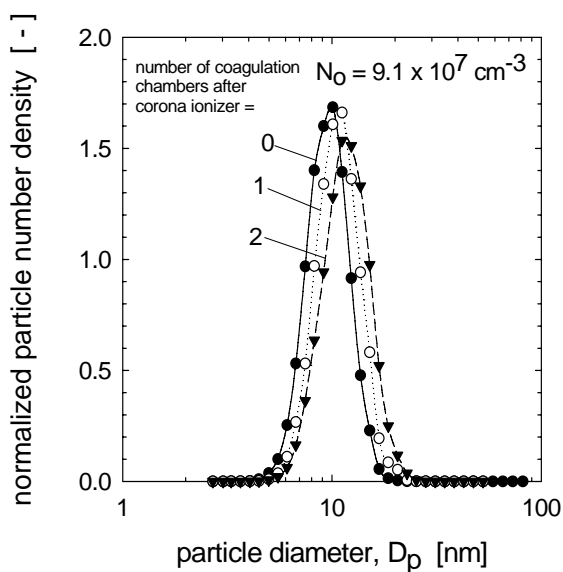


Fig. 10. Size distribution of positively charged particles after the aerosol has passed through 0, 1 and 2 coagulation chambers placed downstream of the corona ionizer. Total aerosol particle number concentration at the ionizer outlet: $9.1 \times 10^7 / \text{cm}^3$.

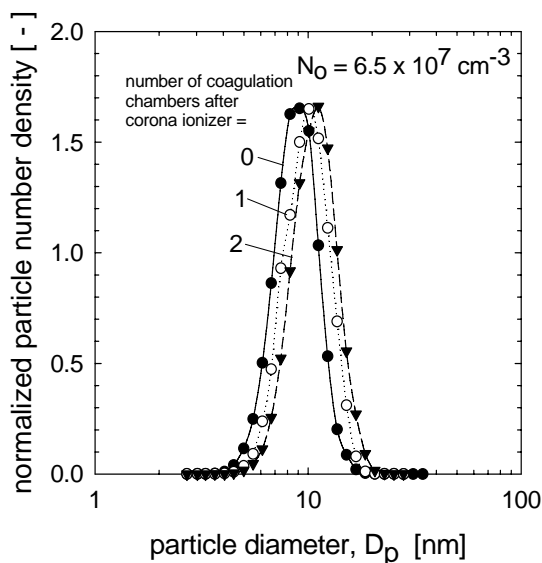


Fig. 11. Size distribution of positively charged particles after the aerosol has passed through 0, 1 and 2 coagulation chambers placed downstream of the corona ionizer. Total aerosol particle number concentration at the ionizer outlet: $6.5 \times 10^7 \text{ cm}^{-3}$.

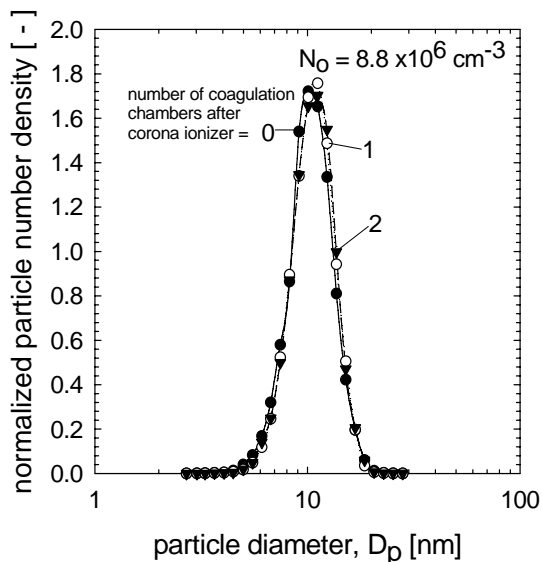


Fig. 12. Size distribution of positively charged particles after the aerosol has passed through 0, 1 and 2 coagulation chambers placed downstream of the corona ionizer. Total aerosol particle number concentration at the ionizer outlet: $8.8 \times 10^6 / \text{cm}^3$.

Table 2. Size distribution of positively charged particles downstream of the ⁸⁵Kr neutralizer. Comparison between experimental results and numerical calculations. D_{pg} = geometric mean diameter; σ_g = geometric standard deviation; N_0 = aerosol particle number concentration at neutralizer outlet; c = number of coagulation chambers after the neutralizer; D_{pg0} , σ_{g0} = particle size distribution parameters at neutralizer outlet. (Mean aerosol residence time in each coagulation chamber = 2.3 s.)

N_0 cm ⁻³	D_{pg0} nm	σ_{g0} (-)	$c = 1$				$c = 2$			
			D_{pg} (nm)		σ_g (-)		D_{pg} (nm)		σ_g (-)	
			exp	calc	exp	calc	exp	calc	exp	calc
6.9×10^7	12.7	1.64	15.1	16.7	1.59	1.60	16.9	17.0	1.56	1.59
4.7×10^7	10.3	1.53	11.5	12.8	1.50	1.49	12.8	13.0	1.48	1.48
8.2×10^6	10.2	1.38	10.1	10.2	1.35	1.37	10.2	10.2	1.34	1.36

Table 3. Size distribution of positively charged particles downstream of the corona ionizer. Comparison between experimental results and numerical calculations. D_{pg} = geometric mean diameter; σ_g = geometric standard deviation; N_0 = aerosol particle number concentration at ionizer outlet; c = number of coagulation chambers after the ionizer; D_{pg0} , σ_{g0} = particle size distribution parameters at ionizer outlet. (Mean aerosol residence time in each coagulation chamber = 2.3 s.)

N_0 cm ⁻³	D_{pg0} nm	σ_{g0} (-)	$c = 1$				$c = 2$			
			D_{pg} (nm)		σ_g (-)		D_{pg} (nm)		σ_g (-)	
			exp	calc	exp	calc	exp	calc	exp	calc
9.1×10^7	9.42	1.26	10.53	10.71	1.27	1.26	11.77	11.74	1.29	1.26
6.5×10^7	8.70	1.26	9.71	9.92	1.26	1.26	10.62	10.81	1.27	1.26
8.8×10^6	10.32	1.27	10.43	10.36	1.26	1.26	10.51	10.39	1.26	1.26

CONCLUSIONS

An experimental comparative study has been carried out to investigate the changes in particle size distribution that can take place in two commercially available aerosol chargers, the TSI ⁸⁵Kr neutralizer model 3077, and the IONER corona charger model CC08010. The main conclusions of this work can be summarized thus: (i) for aerosol concentration above about 10⁷/cm³, particles coagulate in the neutralizer but not in the

corona ionizer; the TSI neutralizer is excessively large. (ii) Coagulation occurs downstream of both types of chargers if the aerosol concentration is, again, higher than about 10⁷/cm³. (iii) The charging-coagulation equations predictions agree well with the experimental results for particle size above 10 nm, but not for particles of a very few nanometers. (iv) The presence of bipolarly charged particles does not affect the coagulation rate, probably because the

fraction of charged particles is not large enough in the size range studied.

REFERENCES

- Adachi, M., Kousaka, Y. and Okuyama, K. (1985). Unipolar and Bipolar Diffusion Charging of Ultrafine Aerosol Particles. *J. Aerosol Sci.* 16: 109-123.
- Alguacil, F.J. and Alonso, M. (2006). Multiple Charging of Ultrafine Particles in a Corona Charger. *J. Aerosol Sci.* 37: 875-884.
- Alonso, M., Kousaka, Y., Nomura, T., Hashimoto, N. and Hashimoto, T. (1997). Bipolar Charging and Neutralization of Nanometer-sized Aerosol Particles. *J. Aerosol Sci.* 28: 1479-1490.
- Alonso, M., Hashimoto, T., Kousaka, Y., Higuchi, M. and Nomura, T. (1998). Transient Bipolar Charging of a Coagulating Nanometer Aerosol. *J. Aerosol Sci.* 29: 263-270.
- Alonso, M., Martin, M.I. and Alguacil, F.J. (2006). The Measurement of Charging Efficiencies and Losses of Aerosol Nanoparticles in a Corona Charger. *J. Electrostatics.* 64: 203-214.
- Buscher, P., Schmidt-Ott, A. and Wiedensohler, A. (1994). Performance of a Unipolar 'Square Wave' Diffusion Charger with Variable nt-product. *J. Aerosol Sci.* 25: 651-663.
- Chen, D.R. and Pui, D.Y.H. (1999). A High Efficiency, High Throughput Unipolar Aerosol Charger for Nanoparticles. *J. Nanoparticle Res.* 1: 115-126.
- Flagan, R.C. and Seinfeld, J.H. (1988). *Fundamentals of Air Pollution Engineering*. Prentice-Hall, Englewood Cliffs.
- Fuchs, N.A. (1964). *Mechanics of Aerosols*. Pergamon Press, New York.
- Gormley, P.G. and Kennedy, M. (1949). Diffusion from a Stream Flowing Through a Cylindrical Tube. *Proc. Royal Irish Acad.* 52A: 163-169.
- Hernandez-Sierra, A., Alguacil, F.J. and Alonso, M. (2003). Unipolar Charging of Nanometer Aerosol Particles in a Corona Ionizer. *J. Aerosol Sci.* 34: 733-745.
- Kousaka, Y., Nomura, T., Alonso, M., Nishio, M. and Tenjiku, E. (2000). Experimental Studies of Gas-phase Nucleation and the Effect of Seed Particles on Homogeneous Nucleation Suppression. *J. Aerosol Sci.* 31: 519-530.
- Kruis, F.E. and Fissan, H. (2001). Nanoparticle Charging in a Twin Hewitt Charger. *J. Nanoparticle Res.* 3: 39-50.
- Qi, C., Chen, D.R. and Greenberg, P. (2008). Performance Study of a Unipolar Mini-charger for a Personal Nanoparticle Sizer. *J. Aerosol Sci.* 39: 450-459.
- Qi, C., Chen, D.R. and Pui, D.Y.H. (2007). Experimental Study of a New Corona-based Unipolar Aerosol Charger. *J. Aerosol Sci.* 38: 775-792.
- Wiedensohler, A., Buscher, P., Hansson, H.C., Martinsson, B.G., Stratmann, F., Ferron, G. and Busch, B. (1994). A Novel Unipolar Charger for Ultrafine Aerosol Particles with Minimal Particle Losses. *J. Aerosol Sci.* 25: 639-649.

Wiedensohler, A., Orsini, D., Covert, D.S., Coffmann, D., Cantrell, W., Havlicek, M., Brechtel, F.J., Russell, L.M., Weber, R.J., Gras, J., Hudson, J.G. and Litchy, M. (1997). Intercomparison Study of the Size-dependent Counting Efficiency of 26 Condensation Particle Counters. *Aerosol Sci. Technol.* 27: 224-242.

Zebel, G. (1966). Coagulation of Aerosols, in *Aerosol Science*, ed. C.N. Davies, Academic Press, London.

Received for review, July 16, 2008

Accepted, September 20x, 2008